

Improved analytical model of the transverse coupling impedance of ferrite kicker magnets

Daniele Davino* and Harald Hahn

Brookhaven National Laboratory, Upton, New York 11973

(Received 19 August 2002; published 9 January 2003)

A transformer model of ferrite kicker magnets is presented in this paper. Based on this model, an equivalent circuit is derived for which the elements can be obtained by bench measurements or by estimates from the magnet geometry. Improved formulas for the transverse coupling impedance of lumped and traveling wave kicker magnets are derived from the model and the equivalent circuit. The formulas differ from the corresponding handbook results in their dependence on the external termination or aperture aspect, respectively. The effect of ferrite properties on the transverse coupling impedance is analyzed. The model was confirmed by bench measurements with the twin-wire technique made on the full-size and half-size prototypes of the extraction kicker of the SNS accumulator ring. The application of this model to the design of the kickers allowed a significant reduction of the SNS transverse coupling impedance budget.

DOI: 10.1103/PhysRevSTAB.6.012001

PACS numbers: 29.27.Bd, 29.27.Ac

I. INTRODUCTION

The transverse coupling impedance of a circular accelerator or storage ring can cause beam instabilities and must be carefully monitored in order to keep its value within the impedance budget. The success of the SNS (Spallation Neutron Source) presently under construction will largely depend on reducing the transverse coupling impedance of the accumulator ring [1]. Next to the resistive wall, the biggest impedance contribution is made by the ferrite kicker magnets. Thus, an extensive experimental and theoretical program was carried out to achieve the design goal, with this paper presenting the paramount results of this study. Although originally directed at solving specific SNS problems, the conclusions are believed to be of more general interest.

The investigations presented here focused on the full-size and half-size prototypes for the SNS extraction kicker magnets. The kicker is built as a window frame magnet and is used to deflect the beam vertically by means of a pulsed magnetic field. The locution “window” refers to the particular setup of ferrite blocks, opening a window where two metallic sheets, i.e., the busbar, create the deflecting magnetic field. The electrical performance of a kicker (magnetic field flatness, magnetic field rise time, and total inductance of the magnet) can be reliably simulated during the design, whereas the coupling impedance can only be roughly estimated by using handbook recipes [2].

The impedance estimates are based on the seminal paper by Nassibian and Sacherer [3] and subsequent reports by Nassibian [4,5], where the expressions for the transverse impedance of lumped and traveling wave kicker magnet are given. Although their formulas have been applied by most workers, for example, to the preliminary measurements of the SNS kicker [6,7], it was recognized that the estimates show general agreement with the real but not with the imaginary part of measured

values [8]. In the frequency range of interest to SNS, the extraction kicker behaves as a lumped kicker for which the transverse impedance estimate is given by Nassibian and Sacherer (hereafter NS) in the notation of this paper

$$Z_{\perp}^{\text{NS}} = \frac{Z_0 l}{hw} \frac{\omega L_2}{j\omega L_2 + Z_g}. \quad (1)$$

The symbols represent the generator impedance Z_g , the impedance of free space $Z_0 = \mu_0 c$, and the nominal magnet inductance $L_2 \approx \mu_0 h l / w$, where the magnet width, height, and length are w , h , and l , respectively. The inadequacy of the formula is most pronounced in the cases of the open and shorted kicker, namely, $Z_g \rightarrow \infty$ and $Z_g = 0$, respectively. In view of the uncertainty regarding the handbook formula, a comprehensive study including bench measurements and further analysis became mandatory.

Bench measurements on the prototype were made using the standard method [9], where the beam is represented by a twin-wire “Lecher” line, which is inserted into the kicker. The forward transmission coefficient of the “device under test” (DUT) is compared to that of the line in a reference beam tube and the resulting changes can be interpreted by established procedures to yield the measured transverse coupling impedance.

Based on the various experimental results described in this paper, an equivalent model of the bench measurements was developed by approximating the kicker as a transformer, in line with the general concepts put forth by NS. In the bench measurements the line and the busbar are linked by a mutual inductance. The coupling of the beam with the busbar is directly described by the beam induced magnetic flux in the kicker structure. One part thereof is coupled to the external circuit via the busbar, but the other part stays concentrated in the local ferrite. The horizontal impedance perpendicular to the kick direction is due to uncoupled flux only. In contrast, the

vertical impedance in the kick direction is dominated by the coupled magnetic flux, with the uncoupled flux giving only a small inductive contribution. This model led to the “improved” expression for the coupled vertical impedance, which is given by

$$Z_y \approx j \frac{Z_0 l}{hw} \frac{Z_g}{j\omega L_2 + Z_g} = \frac{c}{\omega h^2} \frac{j\omega L_2 Z_g}{j\omega L_2 + Z_g} \quad (2)$$

with the symbols as used in the NS formula. Obviously, the new expression differs in the dependence on the external impedance and renders the scaling with aperture height more evident.

In Sec. II of this paper, the impedance model for the impedance due to the *coupled* flux is presented in detail. The experimental justification and the impedance measuring method are described in Sec. III. Complementary measurements yielding the crucial mutual inductance and a simplified impedance measurement performed from the external terminals are given in Sec. IV. In Sec. V, the transformer concept is extended to traveling wave kicker magnets resulting in an improved impedance expression. The paramount properties of the improved impedance model are summarized in Sec. VI. An analytical expression of the impedance due to the *uncoupled* flux is derived in the Appendix.

II. THE IMPROVED IMPEDANCE MODEL FOR LUMPED KICKERS

For the sake of simplifying the impedance analysis, a kicker magnet can be characterized as traveling wave or lumped depending on its electrical length and thus the frequency range considered. The traveling wave kicker has a characteristic impedance intentionally made much smaller than the impedance of free space and the wave propagates much slower than the speed of light. As a result, the electrical length of the kicker must be taken into account, both in the impedance analysis and the bench measurement. In a lumped kicker magnet no effort is made to reduce the characteristic impedance, and it is electrically short. Its impedance model thus is based on the premise that the beam-magnet interaction can be treated like a transformer. The impedance analysis of a lumped kicker is conceptually simpler and is presented first, while the treatment of a traveling wave kicker is postponed until Sec. V. In spite of their different construction, the impedance from the traveling wave and lumped treatment will coincide at sufficiently low frequencies.

The transverse impedance model is here developed for the geometry of a window frame magnet, but the same concepts are applicable to a C-magnet by small changes of the notation. The generic window frame magnet of length l has an aperture width w and has in the kick direction, that is between the plates forming the busbar, an aperture height h .

The transverse coupling impedance of kickers can be measured on the bench by using the standard method in which a twin-wire Lecher line, simulating the beam, is inserted into the DUT. The forward transmission coefficients S_{21}^{DUT} of the kicker are compared with the S_{21}^{REF} obtained in a reference tube of at least equal length and is interpreted according to the Hahn-Pedersen (HP) formula for lumped units [10],

$$Z^{\text{DUT}} \approx 2Z_L(1 - S_{21}^{\text{DUT}}/S_{21}^{\text{REF}})/(S_{21}^{\text{DUT}}/S_{21}^{\text{REF}}), \quad (3)$$

or alternatively the log formula [11],

$$Z^{\text{DUT}} = -2Z_L \log(S_{21}^{\text{DUT}}/S_{21}^{\text{REF}})$$

with Z_L the characteristic impedance of the line. Finally, one obtains the transverse impedance as [12]

$$Z_{\perp} = \frac{c}{\omega} \frac{Z^{\text{DUT}}}{\Delta^2} \quad (4)$$

with Δ being the spacing of the two wires. This relation requires the knowledge of essentially three quantities: the measured impedance of the device under test, the effective wire spacing, and the characteristic impedance. In the typical case of the wire diameter much smaller than the wire spacing, the effective Δ is given by the center-to-center distance of the wires. For wires of diameter d , with center-to-center spacing D , the effective spacing is known to be

$$\Delta = D\sqrt{1 - (d/D)^2}.$$

In all other practical cases, it is necessary to make *ad hoc* measurements of the effective spacing, either by a comparison with a line of known properties or by the mutual inductance measurement described in Sec. IV.

In the bench measurements, the twin-wire line simulates the dipole component of the beam which excites a magnetic flux in the kicker. As discussed in NS, the measured impedance Z^{DUT} has two origins. One part, typically the larger one, is generated by the magnetic flux coupled to the busbar and the external circuit whereas the other, smaller, part represents the contribution from the uncoupled flux. As aid in the interpretation of the impedance measurements, the equivalent circuit for the impedance model in Fig. 1 gives the two contributions explicitly. Note that the Lecher line inductance, L_L , is subtracted by using the reference tube.

In first approximation, the losses of the uncoupled flux can be neglected at very low frequencies for typical ferrites, and the uncoupled impedance can be represented through a simple series inductor, L_s , along the line. The subsequent arguments will prove that the value of this inductor is measured by shorting the busbar. In any case, a small frequency-dependent series resistor can be added to represent the losses.

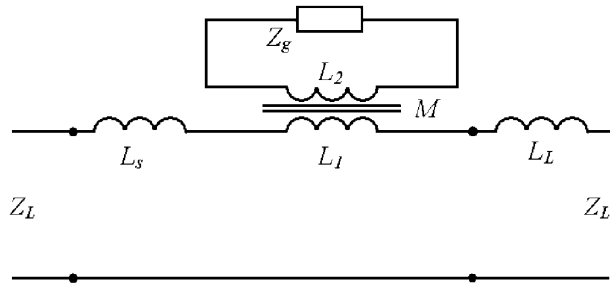


FIG. 1. The low frequency kicker model with the two contributions to the transverse coupling impedance in bench measurements.

The coupled-flux part is usually the main contribution to the transverse impedance and is treated here in detail. Assuming a near perfect ferrite, the flux generated by the current in the busbar is uniformly distributed in the kicker aperture, with a fraction thereof coupled to the twin-wire line. The impedance model of the kicker thus can be represented as a transformer which couples the measuring line with the busbar and the external circuit. The primary side is the twin-wire line, representing the dipolar beam, and the secondary winding is the busbar with the external circuit. It is essential to the present analysis that, for near perfect permeability, the entire busbar generated flux traverses the vertical gap and thus couples via the mutual inductance to the twin-wire line. The absence of a leakage flux on the secondary side makes the coupled-flux part into a perfect transformer. The consequence of a small leakage flux and stray capacity will be discussed in Sec. IVA.

The analysis of the impedance model starts by considering the frequency-domain equations of two coupled inductors:

$$\begin{cases} V_1 = j\omega L_1 I_1 + j\omega M I_2, \\ V_2 = j\omega M I_1 + j\omega L_2 I_2, \end{cases} \quad (5)$$

where M is the mutual inductance and L_2 is the busbar inductance. The inductance, L_2 , can be obtained from the measurement of the input impedance at the busbar. The mutual inductance, M , can be derived from a S_{21} measurement between the twin-wire line and the busbar. Note that L_2 does not depend on the line properties, whereas M does. The perfect coupling condition implies that

$$L_1 = M^2/L_2. \quad (6)$$

The circuit external to the kicker magnet proper is identified by the impedance, Z_g , which represents the feed-through capacitance at the busbar end in parallel with the total external impedance of the feeding cable and the upstream power supply. The secondary voltage of the transformer follows as $V_2 = -I_2 Z_g$. Together with Eqs. (5) and (6), this condition leads to the impedance contribution, Z_1 , from the coupled flux

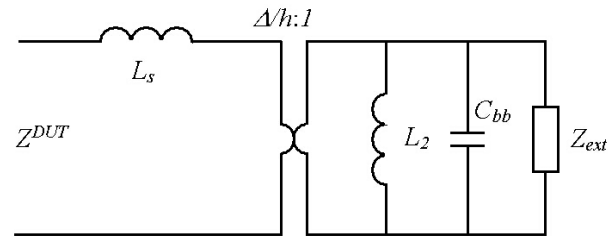


FIG. 2. Equivalent circuit for Z^{DUT} .

$$Z_1 = \frac{V_1}{I_1} = \frac{M^2}{L_2^2} \left(\frac{j\omega L_2 Z_g}{j\omega L_2 + Z_g} \right). \quad (7)$$

In contrast to the NS result, the external impedance Z_g is in parallel with $j\omega L_2$, and then is transformed by an ideal transformer with ratio M/L_2 . Note that the shorted transformer gives no contribution to the measured impedance. This implies that the uncoupled impedance contribution is obtained from a bench measurement when the external circuit is short-circuited as assumed in Fig. 1.

In the present model, using near perfect permeability, the ratio of flux through the measuring line divided by the flux in the gap is in the thin-wire approximation given by

$$\frac{M}{L_2} = \frac{\Delta}{h}. \quad (8)$$

Furthermore, in this model, one finds $L_2 = \mu_0 l h/w$ and $M = \mu_0 l \Delta/w$. It follows that the coupled-flux contribution to the vertical transverse impedance, when measured by a twin wire with spacing Δ , is expressed by

$$Z_y = \frac{c}{\omega \Delta^2} Z_1 = j \frac{Z_0 l}{h w} \frac{Z_g}{j\omega L_2 + Z_g}, \quad (9)$$

the result quoted in the introduction as Eq. (2).

The contribution to the measured impedance Z^{DUT} from the coupled as well as uncoupled flux is pictorially summarized by the equivalent circuit in Fig. 2. The circuit elements represent the inductances L_s obtained from a wire measurement with the busbar shorted. L_2 is directly measured at the busbar, and the capacitance of the busbar C_{bb} can be determined from the possible resonance of the unterminated kicker. Z_{ext} represents the impedance of external components seen at the busbar terminals.

III. EXPERIMENTAL VERIFICATION

A. The SNS extraction kicker

An experimental verification of the proposed impedance model was made by measuring the full-size prototype of one of the 14 SNS extraction kickers with the twin-wire technique. A schematic view of a SNS window frame kicker is shown in Fig. 3. The kicker dimensions are $h = 24.8$ cm, $w = 15.9$ cm, $l = 36$ cm, and $t =$

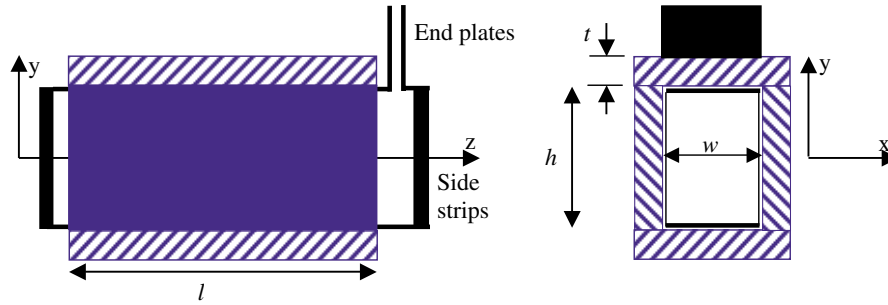


FIG. 3. (Color) Schematic view of a window frame kicker. Crosshatched (blue) frames represent ferrite blocks. z is the beam axis. h is the aperture height, w is the width, l is the busbar length, and t is the ferrite thickness.

2.54 cm. The ferrite type is CMD5005 (Ceramic Magnetics Inc., Fairfield, NJ) and the two busbar plates are connected through side strips. A half-size busbar, with $h = 12.4$ cm, was also made and measured.

Capacitances within the kicker structure must be taken into account because they lead to the resonant behavior. In the SNS kicker case, the main contribution is coming from the busbar end plates which provide the connection to the feedthrough, but the non-negligible permittivity of the ferrite can also make a contribution to C_{bb} coming from the busbar itself. Summing the various contributions leads to an estimated capacity of $C_{bb} = 28.8$ pF for the full-size SNS prototype.

Considering only the magnet part with uniform structure of busbar plates and a ferrite frame, and especially ignoring the capacitance of end plates and feedthrough, leads to the estimate of a magnet inductance of ~ 0.7 μH and capacitance of ~ 10 pF, indicating a characteristic impedance of ~ 245 Ω and a propagation velocity of 65% of light or < 2 ns across the magnet. In the frequency range of interest, that is below 100 MHz, the magnet is indeed a lumped structure.

B. The twin-wire coupling impedance measurement

The twin-wire measurements were performed by using a line, homemade from 5×7.5 mm rectangular tubes, shown in Fig. 4. The center-to-center spacing is 40.6 mm,

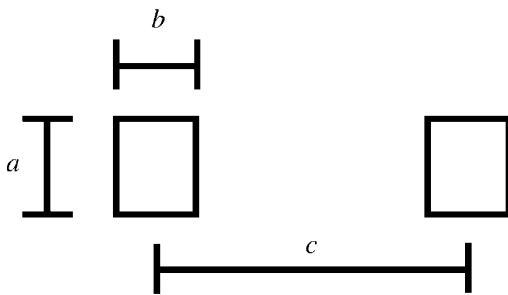


FIG. 4. The homemade cable for the twin-wire measurements. The dimensions are $a = 7.5$ mm, $b = 5$ mm, and $c = 40.6$ mm.

which in good approximation can be taken as Δ for the interpretation of the measurements based on the HP formula. The other value required in the formula, the characteristic impedance of the line, was measured with a communication network analyzer, Tektronix CSA803, to be 260 Ω . Matching of the line characteristic impedance to the 50 Ω cables of the network analyzer, Agilent 8753ES, is achieved by means of 300 Ω transformers (North Hills 0501BB) with a center-tapped secondary winding, serving as a 180° hybrid. The transformer covers the frequencies from 30 kHz up to 100 MHz. The network analyzer was set for a logarithmic frequency range from 100 kHz to 100 MHz, with 1601 points, and a 100 Hz bandwidth. In view of the various measuring errors, a 10%–20% uncertainty in the quoted transverse impedances is expected.

C. Impedance of shorted and open kicker

The bench measurements of the kicker with shorted and open busbar provide, in principle, all data required to establish the kicker model. The real and imaginary part of the measured Z^{DUT} is shown in Fig. 5 left panel for the full-size model, and Fig. 5 right panel shows the measured vertical coupling impedance, Z_y . One can see that the shorted kicker is an inductor and the impedance is almost pure imaginary below 50 MHz. The curve, Z^{DUT}/ω , provides the values of the uncoupled inductance, $L_s \cong 0.025$ μH , and of a frequency-dependent small loss resistor. The same “slope” is found in the imaginary part of the open-termination measurement, but on top of that, there is a resonance at $f = 35$ MHz. This resonance, after subtracting the shorted values and scaling to the busbar side, provides the coupled inductance $L_2 = 0.7$ μH and the capacitance of the busbar end plates, $C_{bb} = 28.8$ pF.

Therefore, the measurements confirm that the short-circuit result represents the part of induced flux that does not couple with the external circuit and the coupled-flux contribution is obtained by subtracting the short-circuit measurement from the open-circuit termination measurement.

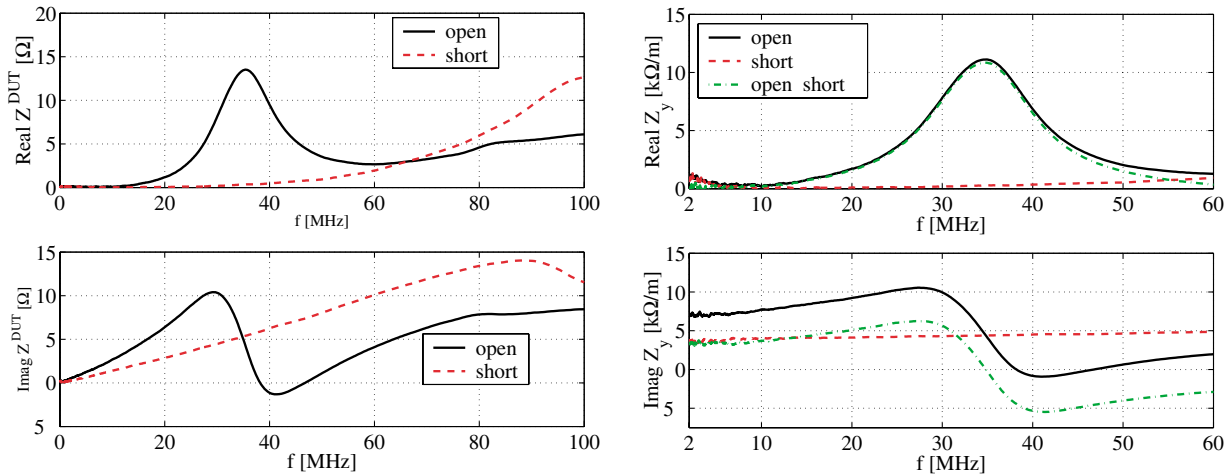


FIG. 5. (Color) Measured kicker impedances, Z^{DUT} (left panel) and Z_y (right panel), with open-circuit and short-circuit terminations at the busbar.

D. Dependence on terminating resistor

The transverse coupling impedance follows from the wire-measured Z^{DUT} by applying Eq. (4) with the nominal wire spacing $\Delta = 45.6$ mm as discussed above. The total impedance must take into consideration the coupled as well as the uncoupled flux. The coupled-flux contribution is separated by subtracting the short-circuit results. The emphasis on the coupled-flux contribution stems from the fact that the beam instabilities are driven by the resistive part, which in turn typically is dominated by the external load via the coupled flux.

In Fig. 6, the typical measurements of the transverse coupling impedance due to the coupled-flux contribution

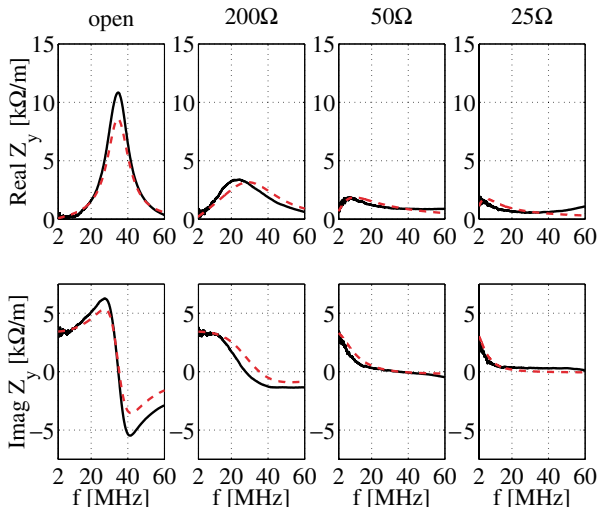


FIG. 6. (Color) Vertical coupling impedance due to the coupled-flux contribution. The solid (black) curves are measured impedances minus the measurement of the short-circuit termination at the busbar and the dashed (red) curves are calculated model values.

for the SNS kicker with resistive terminations are shown [13]. When a resistive termination is applied to the external circuit, the resonant peak is damped. Figure 6 shows the excellent agreement among the fits for 200, 50, and 25 Ω terminations, once the circuit parameters are fitted to the shorted and open-termination measurements. The solid (black) curves represent the measurements and the dashed (red) the theoretical model values.

E. Comparison with the Nassibian and Sacherer formula

It is interesting to compare the open-termination measurements interpreted according to the improved model, Eq. (2), with the NS formula, Eq. (1). In our notation, the NS formula can be expressed as

$$Z_1^{\text{NS}} = \frac{c}{\omega h^2} \frac{\omega^2 L_2^2}{j\omega L_2 + Z_g}. \quad (10)$$

In order to take into account the ferrite losses a $R_2 = 490$ Ω resistor has to be put in parallel with the busbar capacitance, $C_{\text{bb}} = 28.8$ pF, as external termination,

$$Z_g = (1/R_2 + j\omega C_{\text{bb}})^{-1}. \quad (11)$$

In Fig. 7 is shown the comparison of the measured transverse impedance with those from the improved model and the NS formulas, which are all based on the coupled flux only. Note that both models yield essentially the same result for the real part of the impedance, but that the NS formula fails to give the inductive imaginary part at low frequencies, the obvious difference being the hypothesis of perfect coupling of the coupled-flux part in the improved model.

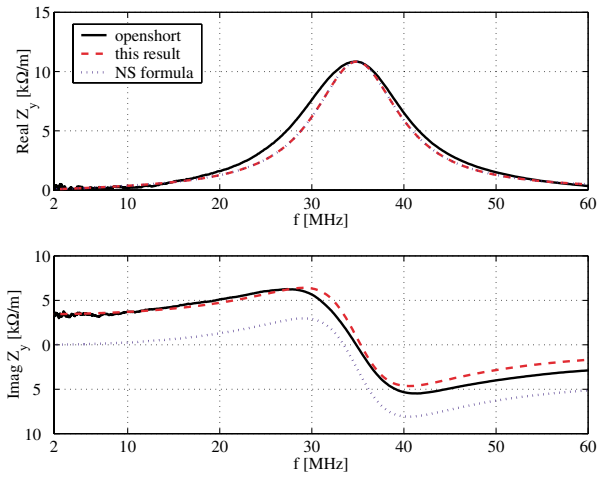


FIG. 7. (Color) Comparison of measurements with improved model and NS formulas.

F. Scaling law

The extraction system of the SNS ring has 14 kickers and the apertures were adjusted with the betatron function to yield the overall SNS ring acceptance [14]. Therefore, a scaling law was needed to estimate the contribution from different kickers to the impedance budget. Following the reasons that led to the improved model formula, Eq. (2), one can write

$$Z_{y2} \cong Z_{y1} \left(\frac{h_1}{h_2} \right)^2. \quad (12)$$

In order to verify this law, a half-size model was assembled with the existing ferrite bricks and a new simplified busbar. In Fig. 8 the measured, the total minus short, impedances are shown for half- and full-size kickers together with equivalent model predictions. In the open-circuit case, on the left side, the resonant frequency of the half-size model is about $\sqrt{2}$ times the full one

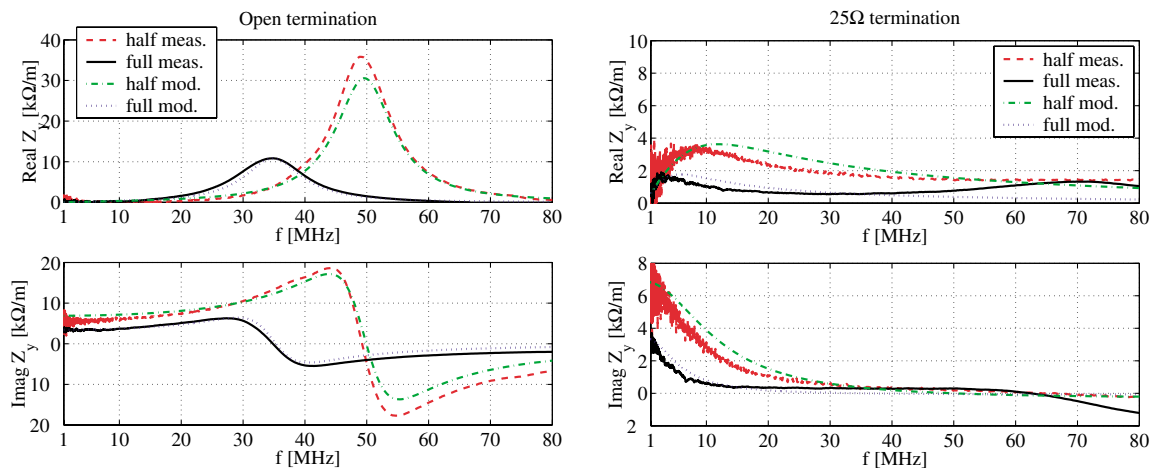


FIG. 8. (Color) Measured (coupled contribution) and predicted impedances for full- and half-size kickers.

because of the halved magnet inductance. The peaks are in good agreement with the application of the equivalent model that gives a factor $4/\sqrt{2}$. It is worth noting that the noisy behavior of all half-size kicker curves in Fig. 8, and the following Figs. 9 and 13, is due only to a higher bandwidth setting for the instrument.

On the right side of Fig. 8, the $25\ \Omega$ termination case also shows a good agreement of measured results with the application of the equivalent model. It is apparent that the scaling law (12) represents a reasonable upper limit to the impedance reduction of kickers that can be expected with increased apertures.

In the SNS extraction system, by taking into account the other constrains (voltage, current, rise time, etc.) to the kickers geometry, a significant reduction was achieved by optimizing the height of the different magnets [15].

G. More detailed model of the kicker

The inductance L_2 in the equivalent circuit of Fig. 2 represents the coupled-flux contribution to the circuit, namely, the busbar inductance of the open magnet. Its value can be obtained from the low frequency limit of the imaginary part of the input impedance measured at the busbar terminals. A small contribution from uncoupled inductances in the busbar, such as the stray inductance due to the side strips connecting the two busbar plates, is here ignored (see Sec. IVA). A more sophisticated model for the busbar contribution, taking into account the ferrite properties, is [16]

$$L_2 = \mu_0 l \frac{h}{w} \frac{\mu_r t}{\mu_r t + h(h/w + 1)}, \quad (13)$$

where t is the thickness of the ferrite bricks and μ_r is the relative permeability, usually expressed as

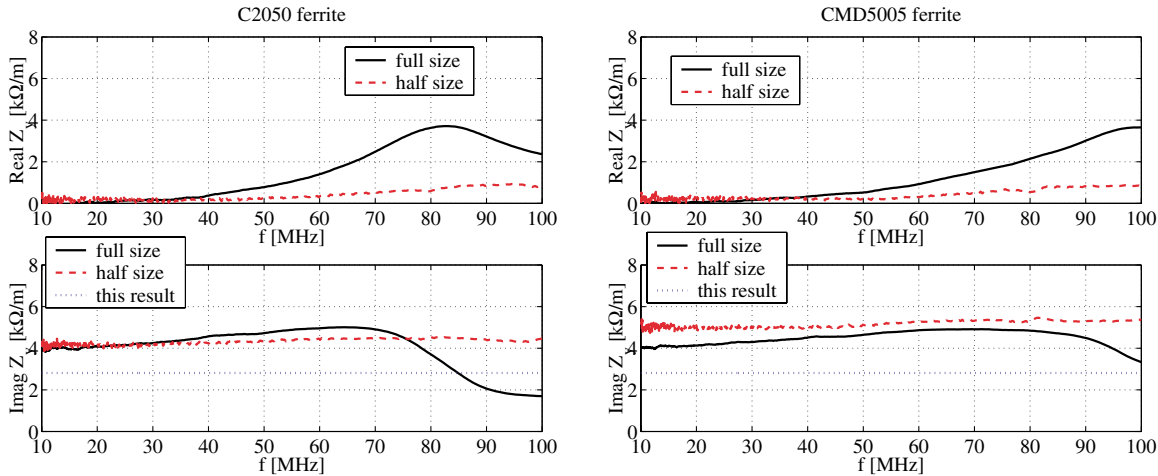


FIG. 9. (Color) Measured transverse impedances with shorted busbar, for half- and full-size kickers, two ferrite types compared with Eq. (15).

$$\mu_r = \mu' - j\mu'' = \frac{\mu_i - 1}{1 + j\omega/\omega_s} \quad (14)$$

with the initial permeability, μ_i , and the saturation frequency, ω_s , obtained from sample measurements. The imaginary part of the permeability gives the losses that can be represented with a frequency-dependent resistor in series with the inductance.

The uncoupled flux can be represented in the equivalent circuit with an inductance L_s , which is in first approximation independent of the aperture height, h . An estimate of the uncoupled impedance is obtained in the Appendix by considering a current dipole between two perfect ferrite plates, leading to

$$Z_{\perp} \approx \frac{j\pi}{6w^2} Z_0 l. \quad (15)$$

For the SNS kicker prototype, the Eq. (15) leads to $Z_{\perp} \cong j2.81 \text{ k}\Omega/\text{m}$ which is in reasonable agreement with the measured values for full- and half-size kickers, as shown in Fig. 9. The theoretical impedance can be interpreted in the equivalent circuit of Fig. 2, with an equivalent inductance $L_s = \mu_0(\pi/6)(l/w^2)\Delta^2 \cong 0.02 \mu\text{H}$ for the SNS prototype. In view of the strong shearing effect, the magnet impedance is only minimally dependent on the ferrite properties. The production SNS magnets are built with the “standard” CMD5005 ferrite.

In estimating the kicker contribution to the impedance budget, the scaling of the uncoupled impedance with horizontal aperture, w , was taken into account.

IV. COMPLEMENTARY MEASUREMENTS

A. Kicker input impedance at the busbar

A direct relation exists between the input impedance, Z_{in} , measured at the busbar port and the coupled contri-

bution to the transverse impedance seen by the beam, and measured by the twin-wire method. Indeed, the measurement of Z_{in} yields the right-hand side of the ideal transformer defined by Fig. 2. In this approximation, an equivalent coupling impedance follows by scaling the input impedance according to

$$Z_{\perp}^{\text{in}} = \frac{c}{\omega h^2} Z_{\text{in}}. \quad (16)$$

This points to the possibility of getting a reasonable idea of the coupling impedance by measuring Z_{in} , especially for kickers mounted in accelerators, provided that an access to the busbar is available. The possibility of obtaining the coupling impedance of an installed magnet by combining external impedance measurements at the kicker terminals with an analytical formula is obviously tempting [17]. However, it must be emphasized that only the coupled-flux contribution is accessible and the coupling impedance perpendicular to the kick direction is not seen.

The input impedance, Z_{in} , is compared in Fig. 10 with the wire-measured coupled impedance contribution, $Z_w = Z_w^{\text{open}} - Z_w^{\text{short}}$ and Z_w^{open} , scaled to the busbar terminal side of the ideal transformer by the ratio $(h/\Delta)^2$. The input impedance of the full-size prototype (left side) shows several resonances, the highest of which is found around 30 MHz, whereas the bench measured impedance has the main resonance around 35 MHz. The imaginary parts of Z_{in} and Z_w at low frequency differ in slopes, indicating different inductances. The inductance from Z_{in} is larger because of the busbar side strips contribution, not considered in the equivalent circuit of Fig. 2. The side strip inductances do not couple with the twin-wire line but can be seen from the busbar terminals. For the full-size prototype of the SNS kicker their contribution can be estimated to be $\sim 0.3 \mu\text{H}$. Furthermore, some parasitic

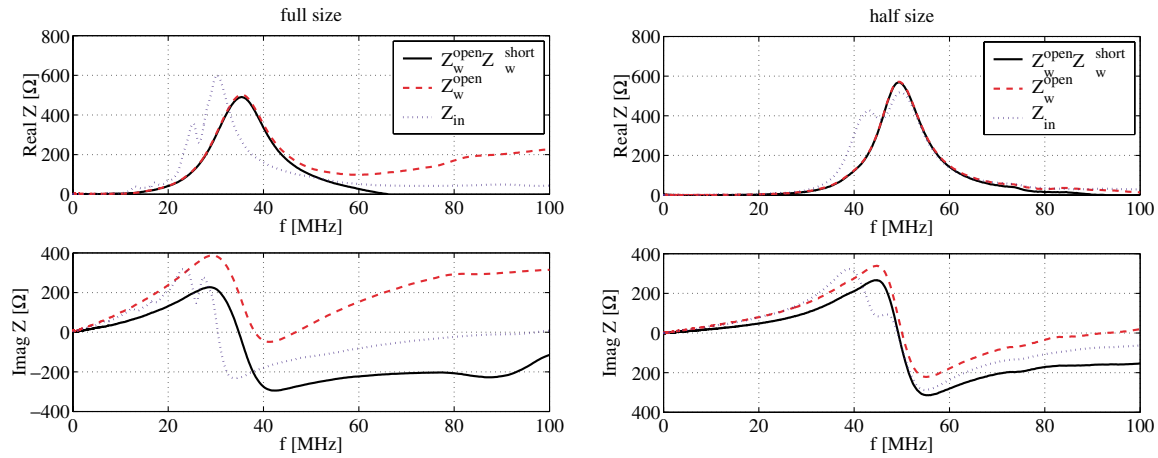


FIG. 10. (Color) Comparison of the input impedance at the busbar and the scaled measured impedance. Full-size model (left panel) and half-size model (right panel).

capacitances are also present, resulting in several small resonances and a lower value of the main resonant frequency at ~ 30 MHz. Similar conclusions can be drawn for the half-size prototype. The comparison of results in Fig. 10 makes it apparent that the two impedances exhibit a similar character and an estimation of the real part is possible, whereas the imaginary part can differ.

B. Mutual inductance measurement

The interpretation of the bench measurements requires the knowledge of the effective wire spacing, Δ , which is linearly dependent on the mutual inductance between the Lecher line and the busbar. Although in a window frame kicker a good estimate of its value can be made, an experimental confirmation is desirable. A method, based on the relation

$$\Delta = h \frac{M}{L_2}, \quad (17)$$

which is also applicable to a more general cross section, e.g., C-magnet, is here suggested.

The Lecher line and the busbar are again considered as a transformer. For this measurement, the Lecher line is without any matching transformers and is shorted at one end. The line now represents the primary of the transformer with the inductance L_L . The busbar is accessed without the feedthrough. The transmission coefficient, S_{21} , from the terminals (index 1) of the Lecher line to the terminals (index 2) of the busbar yields the mutual inductance via simple analytical steps. By considering the arguments of the previous section and the transformer

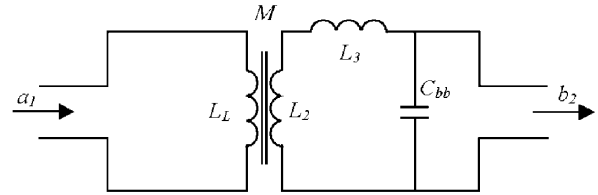


FIG. 11. Transformer model for S_{21} measurement between the twin-wire line and the busbar.

model shown in Fig. 11, and assuming that $M \ll L_L$, $M \ll L_2$, one can write the first relation on the primary transformer side

$$I_1 \approx \frac{2}{Z_N + Z_L} a_1 \quad (18)$$

with a_1 the amplitude of the incoming wave, and $Z_N = 50 \Omega$, the characteristic impedance of the coaxial cables connected to the network analyzer. $Z_L \approx j\omega L_L$ is the input impedance measured at the Lecher line, assuming $M \ll L_L$. The impedance Z_L contains also the uncoupled contribution, but is in this approximation negligible. It is worth noting that I_1 is defined taking into account the reflection coefficient at port 1. A second relation is found on the secondary side,

$$j\omega M I_1 = [1 + j\omega(L_2 + L_3)(Z_N^{-1} + j\omega C_{bb})] b_2. \quad (19)$$

By definition, $S_{21} = b_2/a_1$ and elimination of I_1 yields the expression for

$$\frac{M}{L_2} = \frac{(Z_N + j\omega L_L)[Z_N + j\omega(L_2 + L_3) - \omega^2(L_2 + L_3) C_{bb} Z_N]}{2j\omega L_2 Z_N} S_{21}. \quad (20)$$

This measurement can be compared directly with the estimated geometrical value $\Delta/h \approx 0.366$. Figure 12 shows at low frequency excellent agreement of the measured with the estimated value for the prototypical SNS magnet. The

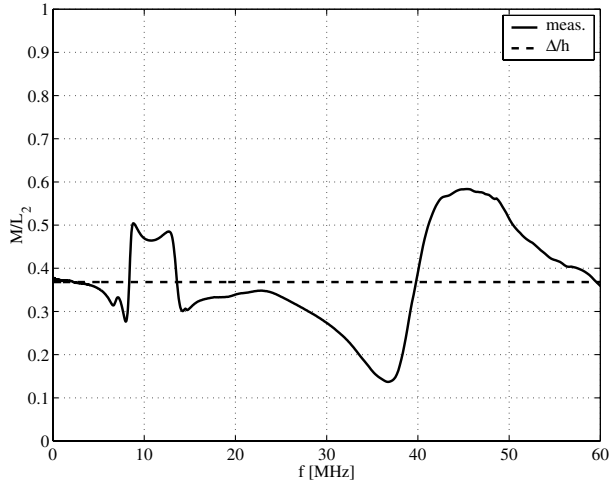


FIG. 12. Comparison of measured value of M/L_2 with estimate for $\Delta/h = 0.366$ for the half-size magnet.

agreement is worse around 35 MHz because of the resonance of the busbar due to its capacitance C_{bb} and various stray capacitances.

C. Horizontal coupling impedance

The horizontal coupling impedance is not coupled to the external circuit via the busbar, and is thus comparable to the uncoupled vertical impedance. Horizontal and vertical coupling impedances for the full- and half-size magnets with the standard ferrite are shown in Fig. 13.

V. THE IMPEDANCE MODEL FOR TRAVELING WAVE KICKERS

The above concept of treating the lumped kicker magnet as a transformer can be generalized and applied to traveling wave kickers. The kicker properties are characterized by its characteristic impedance, Z_K , propagation

constant, k_K , and electrical length, $\Theta = k_K l$. The kicker and the Lecher line are treated as transmission lines, coupled via the mutual inductance, M , for which the differential equations are well known. The general solution becomes unwieldy and several simplifications can be adopted without reducing the value of the results. The major part of the impedance is due to the coupled flux between the beam and the external terminations at either end of the busbar, so that the contribution of the uncoupled flux can be neglected. In order to let the Lecher line represent the “stiff” ultrarelativistic beam, its current is considered externally imposed and thus unchanged by the current in the busbar. The impedance seen by the beam is then obtained by the voltage generated by the busbar current via the mutual inductance. One finds, with the time dependence $e^{j\omega t}$ suppressed, the following set of differential equations in the position dependent variables, i_K , u_K , i_B , and u_B , representing the kicker current and voltage, and the beam current and voltage, respectively

$$\frac{\partial u_K}{\partial s} = -jk_K Z_K i_K + j\frac{\Delta}{h} k_K Z_K i_B, \quad (21)$$

$$\frac{\partial i_K}{\partial s} = -j\frac{k_K}{Z_K} u_K, \quad (22)$$

$$\frac{\partial u_B}{\partial s} = j\frac{\Delta}{h} k_K Z_K i_K, \quad (23)$$

where $k_K = k\sqrt{\langle L \rangle \langle C \rangle}$, $Z_K = \sqrt{\langle L \rangle / \langle C \rangle}$, and $k = \omega/c$. $\langle L \rangle$ and $\langle C \rangle$ are the kicker inductance and capacity per unit length and $\Delta/h = \langle M \rangle / \langle L \rangle$. Assuming an ultrarelativistic beam current, $i_B = I e^{-jks}$, associated with the dipole strength $I\Delta$, one finds the impedance measured in the bench measurement

$$Z^{\text{DUT}} = -2Z_L \ln \frac{S_{21}^{\text{DUT}}}{S_{21}^{\text{REF}}} = -\frac{1}{I} \int_0^l \frac{\partial u_B}{\partial s} e^{jks}. \quad (24)$$

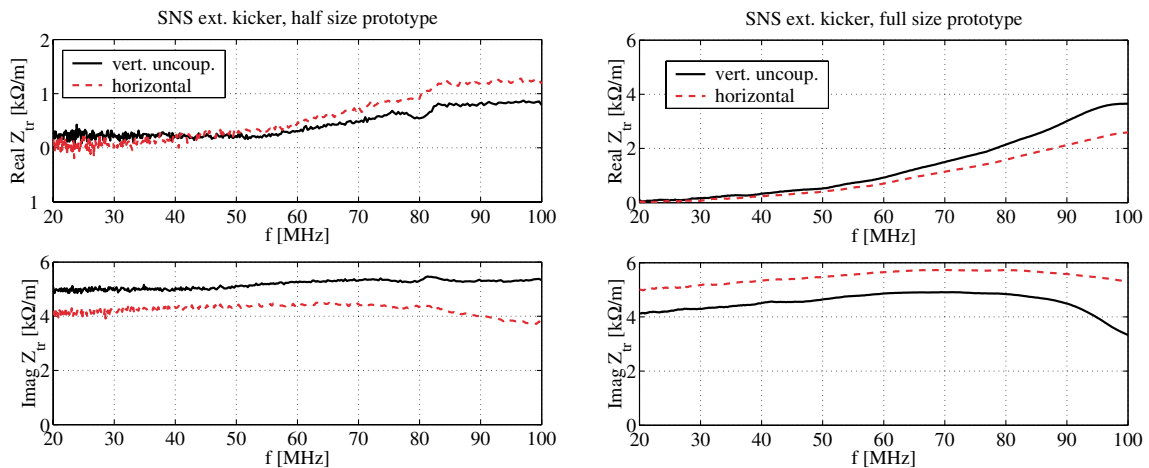


FIG. 13. (Color) Comparison of horizontal and uncoupled vertical impedance of half-size (left panel) and full-size (right panel) magnets.

This value yields the transverse coupling impedance according to

$$Z_{\perp} = \frac{c}{\omega \Delta^2} Z^{\text{DUT}}. \quad (25)$$

The solutions of the above differential equations are found by imposing the boundary conditions established by the kicker input and output terminations, R_i and R_o ,

$$u_K(0) = R_i i_K(0), \quad (26)$$

$$u_K(l) = -R_o i_K(l). \quad (27)$$

The general expression for the coupling impedance is somewhat lengthy, but reduces in typical kickers where $k \ll k_K$ to a manageable size. Furthermore, in the low frequency range of interest, one can take $i_B \approx I$. The case of input and output terminated with the characteristic impedance follows in this approximation as

$$Z_{\perp} = \frac{c}{\omega h^2} Z_K [(1 - \cos\Theta) + j(\Theta - \sin\Theta)], \quad (28)$$

which differs from Nassibian's expression [18]

$$Z_{\perp}^{\text{NS}} = \frac{c}{\omega w^2} Z_K [(1 - \cos\Theta) + j(\Theta - \sin\Theta)] \quad (29)$$

only in its dependence on geometry. (Note that the corresponding handbook formula contains typographical errors [19].)

VI. SUMMARY

The improved kicker model analyzes the total coupling impedance in terms of contributions from the uncoupled flux and the flux coupled to the external circuit. The coupled impedance represents the dominant part as seen in the SNS example of Fig. 5 and thus is the main focus of this paper. The present model leads to a general formula that states a more accurate correlation between the coupling impedance of window frame magnets and its parameters, such as geometric dimensions, external circuit impedance, and ferrite characteristics. It can be used as a guide to the design of kickers in high intensity machines where the coupling impedance budget is a concern. Although based on a lumped window frame magnet, the results are applicable to more general geometries, in particular, the C-magnet. The model can be used in different ways.

The fit from two bench wire measurements of the magnet, with the external circuit open and short-circuited, gives all the circuit elements. The circuit can then be used to calculate the impedance with respect to any external load.

The dominant elements of the equivalent circuit can be obtained from the dimensions of the magnet with busbar and the ferrite properties. The analytical formulas, in particular, the geometric scaling laws, can then be

used to predict and minimize the magnet transverse impedances.

A measurement of the input impedance from the external kicker terminals leads to the fit of the major part of the equivalent circuit, and together with the analytical impedance formula allows estimates of the resistive kicker impedance and the coupled part of the imaginary impedance. The other component, not coupled with the external circuit and usually less important for the coupling impedance, can be approximated by an analytic formula.

ACKNOWLEDGMENTS

The authors acknowledge support from the SNS project. SNS is managed by UT-Battelle, LLC, under Contract No. DE-AC05-00OR22725 for the U.S. Department of Energy. SNS is a partnership of six national laboratories: Argonne, Brookhaven, Jefferson, Lawrence Berkeley, Los Alamos, and Oak Ridge.

APPENDIX: ESTIMATE OF THE UNCOUPLED IMPEDANCE

A qualitative estimate of the uncoupled vertical impedance of the kicker is here derived for the simple model of a dipole between two perfect ferrite plates, spaced apart by the width w . The results are obtained under the assumption that the impedance is independent of the aperture height, that the fields can be treated as two dimensional, and that only the magnetic field is changed by the ferrite plates.

The electric field components in free space generated by a vertical dipole moment, $I\Delta$, representing currents I at $y = \pm\Delta$, are

$$E_{y\infty} = -Z_0 \frac{I\Delta}{\pi r^2} \cos\varphi, \quad (A1)$$

$$E_{x\infty} = Z_0 \frac{I\Delta}{\pi r^2} \sin\varphi. \quad (A2)$$

The magnetic field of the dipole between the perfect ferrite plates is found by conformal mapping, based on $F = \tan(x - \pi/2 + jy)$ [20], as

$$H_{x\mu} = \frac{\eta^2 I\Delta}{2\pi} \frac{(2 \cos 2\eta x \cosh 2\eta y - 1)}{(\sinh^2 \eta y + \sin^2 \eta x)^2}, \quad (A3)$$

$$H_{y\mu} = \frac{\eta^2 I\Delta}{2\pi} \frac{\sin 2\eta x \sinh 2\eta y}{(\sinh^2 \eta y + \sin^2 \eta x)^2}, \quad (A4)$$

with $\eta = \pi/w$. The vertical coupling impedance per unit length follows from the general definition

$$Z_{\perp} = \frac{j}{2I\Delta} (E_y - c\mu_0 H_x). \quad (A5)$$

An approximate expression is now found by Taylor

expansion of $(E_{y\infty} - Z_0 H_{x\mu})_{y=0}$ with respect to x , and retaining only the value at $x = 0$, leading to

$$Z_{\perp} \approx \frac{j\pi}{6w^2} Z_0. \quad (\text{A6})$$

This result leads to the theoretical value of the equivalent uncoupled inductance L_s in the circuit of Fig. 2,

$$L_s = \mu_0 \frac{\pi}{6} \frac{l}{w^2} \Delta^2. \quad (\text{A7})$$

It is worth noting that this expression depends on the wire spacing Δ , whereas the uncoupled impedance is an intrinsic property of the magnet and is obviously independent of Δ . Application of Eq. (4) to $Z^{\text{DUT}} = (j\omega L_s + \dots)$ recovers the intrinsic impedance value.

*Now at: Dipartimento di Ingegneria, Università del Sannio, Piazza Roma, 82100 Benevento, Italy.

- [1] J. Wei *et al.*, Phys. Rev. ST Accel. Beams **3**, 080101 (2000).
- [2] *Handbook of Accelerator Physics and Engineering*, edited by A.W. Chao and M. Tigner (World Scientific, Singapore, 1998), p. 206.
- [3] G. Nassibian and F. Sacherer, Nucl. Instrum. Methods **159**, 21–27 (1979).
- [4] G. Nassibian, CERN Report No. PS 84-25, 1984.
- [5] G. Nassibian, CERN Report No. 85-68 (BR), 1986.
- [6] J.G. Wang and S.Y. Zhang, Nucl. Instrum. Methods Phys. Res., Sect. A **459**, 381–389 (2001).
- [7] S.Y. Zhang, BNL Report No. C-A/AP/20, 2000, http://www.agsrhichome.bnl.gov/AP/ap_notes/ap_note_20.pdf
- [8] H. Hahn and D. Davino, in *Proceedings of the Particle Accelerator Conference, Chicago, 2001*, edited by P.W. Lucas and S. Webber (IEEE, Piscataway, NJ, 2001), p. 1829.
- [9] F. Caspers, in *Handbook of Accelerator Physics and Engineering* (Ref. [2]), p. 571.
- [10] H. Hahn, Phys. Rev. ST Accel. Beams **3**, 122001 (2000).
- [11] L.S. Walling, D.E. McMurry, D.V. Neuffer, and H.A. Thiessen, Nucl. Instrum. Methods Phys. Res., Sect. A **281**, 433–447 (1989).
- [12] L.S. Walling, D.E. McMurry, D.V. Neuffer, and H.A. Thiessen, Nucl. Instrum. Methods Phys. Res., Sect. A **281**, 433–447 (1989).
- [13] D. Davino, H. Hahn, and Y.Y. Lee, in *Proceedings of the 2002 European Particle Accelerator Conference, Paris, France* (CERN, Geneva, 2002), pp. 1467–1469.
- [14] N. Tsoupas *et al.*, in *Proceedings of the 2000 European Particle Accelerator Conference, 2000, Vienna, Austria*, edited by M. Regler (European Physical Society, Geneva, 2000), p. 2270.
- [15] D. Davino, J.L. Mi, and N. Tsoupas, BNL, BNL/SNS Technical Note No. 112, 2002, <http://server.c-ad.bnl.gov/esfd/bnlsns/112.pdf>
- [16] H. Hahn and D. Davino, in *Proceedings of the 2002 European Particle Accelerator Conference, Paris, France* (Ref. [13]), pp. 1502–1504.
- [17] U. Blell, in *Proceedings of the Particle Accelerator Conference, New York, 1999*, edited by A. Luccio and W. MacKay (IEEE, Piscataway, NJ, 1999), p. 1727.
- [18] G. Nassibian, CERN Report No. PS 84-25, 1984.
- [19] K.Y. Ng, in *Handbook of Accelerator Physics and Engineering* (Ref. [2]), p. 206.
- [20] W. von Koppenfels and F. Stallmann, *Praxis der konformen Abbildung* (Springer-Verlag, Berlin, 1959), p. 81.